Polymer and Sphere Diffusion in Confinement

by Malancha Gupta

B.E., Chemical Engineering, The Cooper Union

Submitted to the Department of Chemical Engineering in Partial Fulfillment of the Requirements for the Degree of

MASTER OF SCIENCE IN CHEMICAL ENGINEERING

at the

MASSACHUSETTS INSTITUTE OF TECHNOLOGY

November 2004 [February 2005]

Signature of Author:

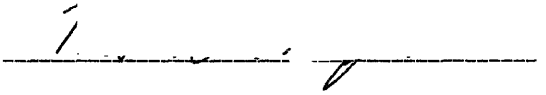

Malancha Gupta

Department of Chemical Engineering

November 3, 2004

Certified by:

Professor Patrick S. Doyle

Thesis Supervisor

Accepted by:

Daniel Blankschtein

Professor of Chemical Engineering

Chairman, Committee for Graduate Studies

Abstract

We use video microscopy and particle tracking to study the diffusion of both colloidal spheres and polymers in slit microchannels. The molecules are allowed to sample the entire height of the microchannel. We find that the sphere data agrees well with a gap-averaged Oseen linear superposition approximation even at very high confinement whereas polymer chains at high confinement can not be modeled by this far field approach. We find that the polymer chain dynamics at high confinement can be explained well by a blob model scaling.

I. INTRODUCTION

The dynamic behavior of macromolecules in confinement is of great interest in various fields. Many current experimental techniques implement lab-on-chip devices in which polymers and spheres are enclosed in small devices. For example, DNA separation is performed in capillaries, nanochannels, and microchannels [1, 2]. Many current drug delivery methods involve the diffusion of solutes through confined spaces such as skin pores [3] and arteries [4, 5]. Characterizing how the dynamic behavior of macromolecules change upon being confined will help us understand and optimize these procedures.

The diffusion coefficient of a sphere in free solution can be found from the Stokes-Einstein relation:

$$D_\infty = \frac{kT}{6\pi\mu R} \tag{1}$$

Deviations from equation 1 occur when there is a boundary close to the sphere. This is a hydrodynamic effect. As the sphere gets close to the boundary, its drag force increases since the velocity at the wall must go to zero. The drag force on a particle near a boundary can be derived using the method of reflections. This far field approach has been successful in predicting the drag force on a particle near a single wall but the drag force on a particle diffusing between two walls is more complicated and has been studied extensively. Faxen was able to find analytical solutions only for the cases where a particle was located in the mid-plane or quarter-plane between the two walls [6]. The Oseen linear superposition approximation has been used to estimate the two-wall drag coefficient in other geometries. In this approximation, the drag coefficient due to two walls is approximated by the sum of two single wall drag coefficients [7]. The disadvantage of this approximation is that it violates the boundary conditions at both walls. Lobry and Ostrowsky [8] tried to satisfy the no-slip boundary condition on both walls by using an infinite superposition of single-wall effects in which backflows were accounted for. They found good agreement with their dynamic light scattering experiments. Lin et al. [9] used optical tweezers to position a sphere at differing heights between parallel walls in order to track its height-dependent dynamic properties. They found that the Oseen linear superposition approximation and Faxen's result at the mid-plane agreed better with their experiments than the infinite superposition approximation. Dufresne et al. [7] also used optical tweezers experiments and found that the Oseen linear superposition approximation was fairly accurate in predicting the diffusion coefficient at small separations.

Although the far field approach can be used to study particles of any shape, it has primarily been used to study spheres. The dynamics of confined polymers chains has only been studied in detail using polymer scaling laws. Brochard and de Gennes [10] used a blob model to derive the scaling law for the diffusion of a polymer chain confined in a tube or slit. Recently Chen et al. [11, 12] used Brownian dynamics simulations with hydrodynamic interactions (BD-HI) to study how DNA chains diffuse in square and slit microchannels. The DNA chains were represented as N_b beads connected by N_s=N_b-1 wormlike chain springs. The lengths of the DNA and the heights of the channels were varied. In the highly confined region, it was found that the diffusivity of the polymer chains were in close agreement with the scaling predicted by the blob model.

In this study we will we use video microscopy and particle tracking to study the diffusion of both colloidal spheres and polymers in slit microchannels. We will compare our results to the Oseen linear superposition approximation in order to verify whether the diffusivity of both spheres and polymer chains can be predicted using a far field approach. Since our molecules will be allowed to diffuse throughout the entire height of the channel, we will compare our results to both a gap-averaged and non-averaged Oseen approximation. We will also compare our polymer data to the blob model scaling and recent simulations.

II. THEORY

The derivation of the first-order effect of boundaries on the drag force of a particle translating with velocity U is treated in Happel and Brenner [6]. The core of the analysis utilizes the linearity of Stokes' equations and the boundary conditions to represent the velocity and pressure fields as a sum of solutions where each solution is found by the method of reflections. The initial velocity field corresponds to the motion of the particle in free solution. This initial field is calculated by assuming that the particle generates the same field as that which would be produced by a point force of strength F_∞ situated at the center of the particle where F_∞ is the free solution drag force on the particle. This far field approach has the advantage that it can be applied to particles of any shape. The diffusion coefficient of a particle located a distance z away from the boundary is found to be:

$$\frac{D(z)}{D_\infty} = 1 - \frac{kF_\infty}{6\pi\mu U z} \tag{2}$$

where k is a dimensionless constant that depends on the type of boundary. Substituting $F_\infty = 6\pi\mu UR$ for a sphere and k=9/16 for a particle moving parallel to a single plane wall yields the diffusion coefficient of a sphere moving parallel to a single plane wall D_1:

$$\frac{D_1(z)}{D_\infty} = 1 - \frac{9R}{16z} \tag{3}$$

For a sphere moving parallel between two plane walls, Faxen was able to find analytical solutions only for the cases where a sphere was located in the mid-plane or quarter-plane between the two walls [6]. The Oseen linear superposition approximation has been used to estimate the diffusion coefficient in other geometries. In the Oseen approximation, the drag coefficient ξ_2 due to two walls is approximated by the sum of two single wall drag coefficients [7]:

$$\xi_2(z) = \xi_\infty + [\xi_1(z) - \xi_\infty] + [\xi_1(H - z) - \xi_\infty] \tag{4}$$

where ξ_∞ is the free solution drag coefficient and ξ_1 is the single wall drag coefficient. Since the diffusion coefficient is inversely proportional to the drag coefficient, equation 4 may be rewritten in terms of a two-wall diffusion coefficient D_2:

$$D_2(z) = \frac{kT}{\xi_2(z)} \tag{5}$$

Lin et al. [9] and Dufresne et al. [7] used optical tweezers to position spheres at fixed heights between parallel walls and found good agreement with the Oseen linear superposition approximation. In our experiments the sphere does not stay at a fixed height but instead samples the entire gap height. In this case, equation 5 should be integrated to yield a gap-averaged two-wall diffusion coefficient $\langle D_2 \rangle$:

$$\langle D_2 \rangle = \int_R^{H-R} \frac{kT}{\xi_2(z)} P(z) dz \tag{6}$$

where $P(z)$ is the probability density distribution.

Since Equations 2-6 were derived using a far field approach, theoretically these equations can be applied to polymer chains as long as the sphere radius is replaced by the hydrodynamic radius of the polymer chain. This hydrodynamic radius is the radius of a sphere that has the same free solution drag force (F_∞) as the polymer chain.

Polymer scaling laws can also be used to estimate the effect of boundaries on the diffusion of polymer chains. The free solution radius of gyration of a polymer chain in a good solvent scales as $R_g \sim bN^{\frac{3}{5}}$ where N is the number of Kuhn steps and b is the Kuhn length. A polymer chain is confined when $2R_g$ is greater than the gap height. Brochard and de Gennes

used a blob model to derive the scaling law for diffusion in this confined region [10]. In the blob model, the polymer chain is represented as a row of blobs of diameter H. Each blob contains g monomers where g is defined by $H \sim b g^{\frac{3}{5}}$ and the number of blobs, N_{blob}, in the chain is therefore $\frac{N}{g} \sim \left(\frac{R_g}{H}\right)^{\frac{5}{3}}$. The hydrodynamic interactions between the blobs are strongly screened and the total drag on the polymer chain is the sum of the drag on each blob:

$$\xi_{total} \sim H N_{blob} \sim H \left(\frac{R_g}{H}\right)^{\frac{5}{3}} \tag{7}$$

The dimensionless scaling law for the diffusion of a confined polymer chain using the blob model is therefore:

$$\frac{\langle D_2 \rangle}{D_\infty} \sim \left(\frac{R_g}{H}\right)^{-\frac{2}{3}} \tag{8}$$

III. EXPERIMENTAL

λ-phage DNA (48502 base pairs) was used as the model polymer in this study. λ-phage DNA has a contour length of 16.3μm and a diameter of 2nm. Longer DNA chains were created by concatenating λ-phage DNA using T4 DNA ligase. The DNA (0.36μg/mL) was labeled with TOTO dye at a concentration of 1 dye molecule per 4 base pairs. Labeling at this ratio increases the contour length of λ-phage DNA from 16.3μm to 21μm [13]. Carboxylated polystyrene beads with radius sizes between 0.055μm and 0.463μm were purchased from Polysciences, Inc. Microchannels were made by pouring polydimethylsiloxane (PDMS) over a silicon wafer containing a photoresist projection of the channel. The mold was heated at 60^{o}C for five hours and then the channels were cut and soaked in filtered 0.5X TBE (Tris Base, Boric Acid, and EDTA) overnight at 50^{o}C in order to prevent flow caused by solvent permeation into the PDMS [14]. Before insertion into the channel, the stained DNA was diluted five times into a final concentration of 4% β-mercatopethanol, 0.1% ascorbic acid, 10mM NaCl, and 0.5X TBE. β-mercaptoethanol and ascorbic acid protect the DNA from free oxygen radicals and NaCl sets the persistence length to 50nm and reduces the Debye length to 2.2nm. The DNA experiments were conducted at a temperature of 294K at which the buffer had a viscosity of 1.08cP. The polystyrene beads (2.5% aqueous suspension) were diluted using 0.5X TBE and 2mM NaCl (0.98cP) into a final concentration of 0.004% aqueous suspension. A small drop of the diluted molecules was placed next to each end of the microchannel and the microchannel proceeded to fill by capillary action. The ends of the microchannel were then sealed with vaseline in order to stop flow. Figure 1 shows the

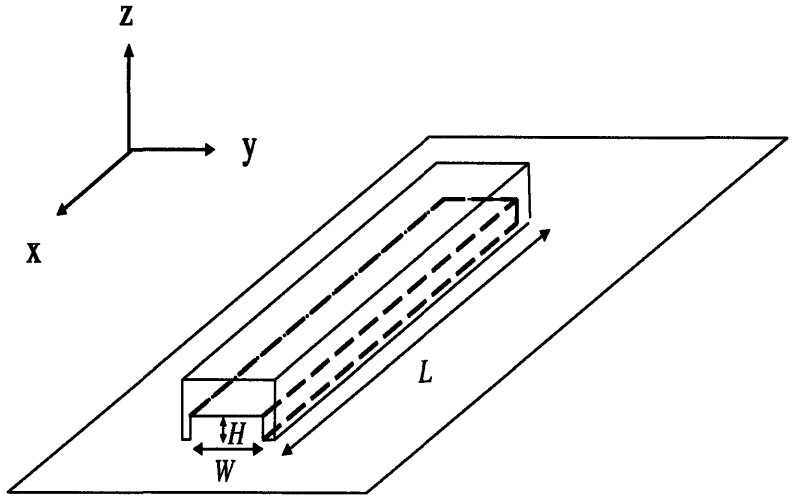

FIG. 1: Setup of the microchannel. The bottom of the channel is attached to a glass coverslip.

orientation of the microchannel. The microchannels had a width of 50μm, a length of 3cm, and a height of either 1.3μm, 2.14μm, or 2.7μm. Only molecules at least 15μm away from the side walls were analyzed in order to neglect the effects of the side walls.

The x-y plane of the channel was observed using a Zeiss Axiovert 200 inverted microscope with a 100X, 1.4 NA oil immersion objective. The images were captured with a Hamamatsu EBCCD camera and analyzed using custom macros written in NIH Image. The macros first subtracted out the background noise and then the x- and y-coordinates of the center of mass of the molecule were found from the first moment of the intensity distribution. Since the molecules were not fixed at a certain height but instead sampled the entire height, the two-wall gap-averaged diffusion coefficient $\langle D_2 \rangle$ could be found from the mean squared displacement of the center of mass :

$$\langle \Delta x^2(\tau) \rangle + \langle \Delta y^2(\tau) \rangle = 4 \langle D_2 \rangle \tau \tag{9}$$

where τ is the lag time. Figure 2 compares the mean squared displacements for the x- and y-directions. The x-direction gap-averaged diffusion coefficient was found to be 0.162μm^2/s and the y-direction gap-averaged diffusion coefficient was found to be 0.160μm^2/s. The error between these diffusion coefficients is only $\sim$ 1.25%. It can be concluded that the gap-averaged diffusion coefficients in the x- and y-directions are the same as long as the flow along the length of the channel is stopped with vaseline and only molecules at least 15μm away from the side walls are observed.

The free solution diffusion coefficients of λ, 2-λ, or 3-λ DNA were found by placing the

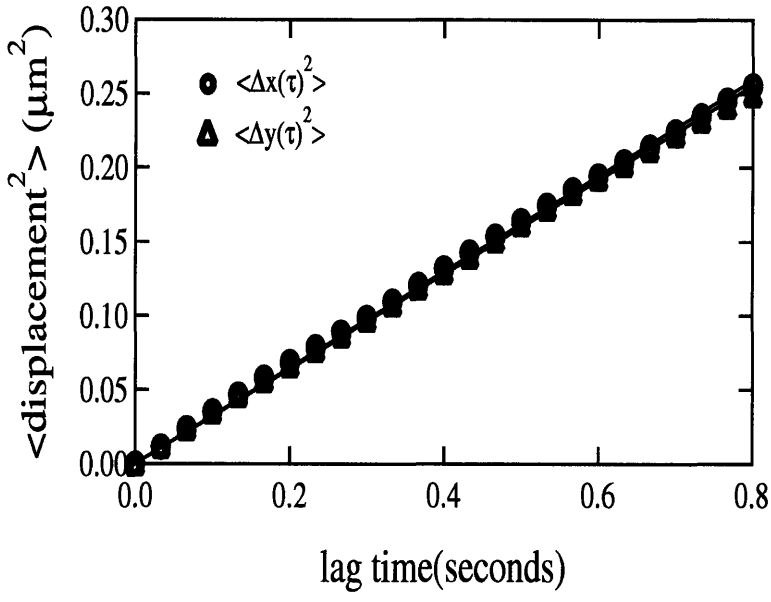

FIG. 2: Mean squared displacement versus lag time for 2-λ DNA diffusing in a 1.3μm high channel. Twelve molecules were tracked for 10 seconds each. The gap-averaged diffusion coefficient in each direction was found from the slope of the linear fit (slope=$2\langle D_2 \rangle$). The x-direction gap-averaged diffusion coefficient was found to be 0.162μm^2/s and the y-direction gap-averaged diffusion coefficient was found to be 0.160μm^2/s.

DNA between two coverslips separated by several hundred microns. In order to neglect the effect of the coverslips, only molecules at least 20μm away from the coverslips were tracked. The free solution diffusion coefficients of the beads were found using the Stokes-Einstein relation (equation 1).

In order to verify whether a DNA molecule was an intact λ, 2-λ, or 3-λ DNA, the time-averaged total intensity of the molecule $\langle I \rangle_{mol}$ and time-averaged radius of gyration of the molecule $\langle R_g \rangle_{mol}$ were calculated using the intensity distribution. Intensity is linearly proportional to mass and therefore all DNA molecules of the same size should have the same $\langle I \rangle_{mol}$ within error. Since intensity varied slightly between experiments due to inherent experimental and instrumental error, $\langle I \rangle_{mol}$ was normalized by dividing by $\langle \langle I \rangle_\lambda \rangle$, the ensemble average of $\langle I \rangle_\lambda$ in that particular experiment. Intact λ, 2-λ, and 3-λ therefore had a normalized intensity of 1, 2, and 3 respectively regardless of the particular experiment. In order to further ensure that the molecules were indeed intact λ, 2-λ, or 3-λ DNA, $\langle R_g \rangle$ was found from the second moment of the intensity distribution and was compared to the free

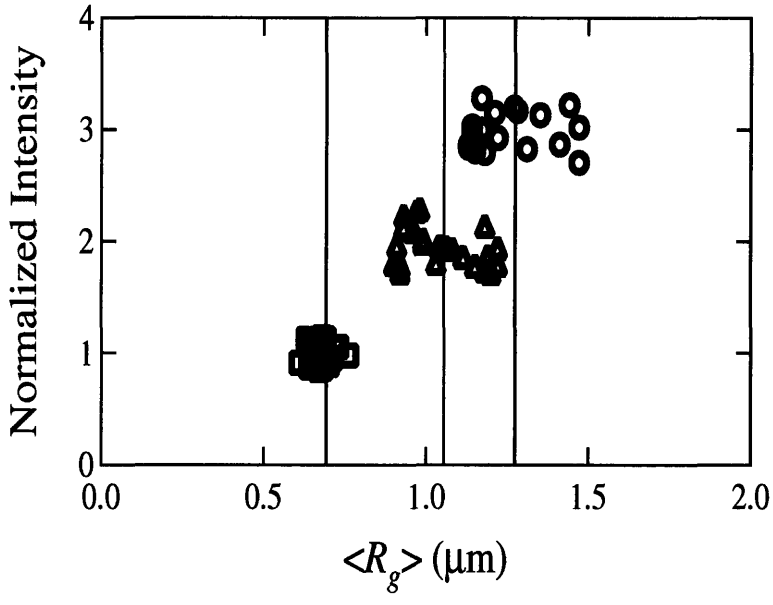

FIG. 3: Normalized intensity versus the average radius of gyration. The data for λ, 2-λ, and 3-λ DNA are represented by squares, triangles, and circles respectively. Each symbol represents a different molecule. The lines through the data represent the values of the free solution radius of gyration found using the free solution diffusion coefficient in the Zimm model for a polymer in a good solvent (equation 10).

solution R_g found using the experimental D_∞ in the Zimm model for a polymer in a good solvent [15]:

$$D_\infty = \frac{0.192kT}{\sqrt{6}\mu R_g} \tag{10}$$

The free solution R_g found using equation 10 was 0.69μm, 1.06μm, and 1.27μm for λ, 2-λ, and 3-λ DNA respectively. Figure 3 shows the plot of the normalized intensity versus the average radius of gyration for intact molecules. The data form disk-shaped clusters that become wider as the DNA gets longer. The scatter in the $\langle R_g \rangle$ data for longer DNA is to be expected since the relaxation time of a polymer in a good solvent scales as $L^{1.8}$ and therefore less configurations can be sampled for 3-λ DNA than for λ DNA in the same amount of observation time. For each experiment approximately 15 molecules were tracked for 10 seconds each.

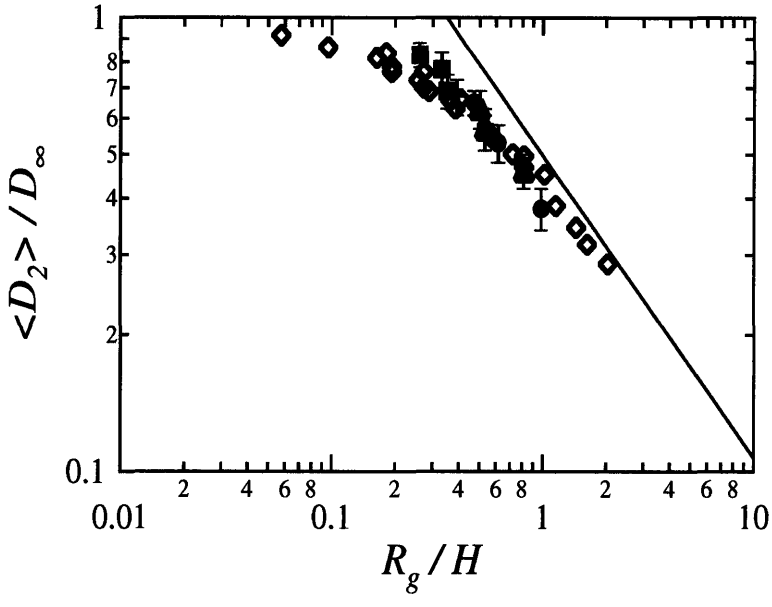

FIG. 4: Normalized gap-averaged diffusion coefficient versus normalized height of the channel for DNA. The experimental data for λ, 2-λ, and 3-λ DNA are represented by filled squares, triangles, and circles respectively. The simulation results are shown in diamonds [11]. The solid line represents the $-\frac{2}{3}$ blob model scaling (equation 8).

IV. RESULTS

Figure 4 shows a plot of the experimental data for DNA on a dimensionless plot of $\langle D_2 \rangle / D_\infty$ versus R_g/H. The results collapse onto a master curve. Error bars were found by dividing the data into five smaller groups and calculating the standard deviation. Figure 4 also shows the simulation data for slit channels by Chen et al. [11]. It can be seen that the experimental data agrees with the simulation data to within error and both data sets appear to follow the highly confined $\langle D_2 \rangle / D_\infty \sim (R_g/H)^{-\frac{2}{3}}$ scaling predicted by the blob theory when R_g/H >0.3. There is a slight difference between the simulations and experiments in the region where the DNA chains first become highly confined (R_g/H ~0.25). In this crossover region, the simulations predict a lower diffusivity than that found from the experiments. This lower diffusivity may be the result of overestimating the effect of the wall in the simulations [11].

Figure 5 shows the experimental data points for the polystyrene beads. In order to compare these results to the gap-averaged Oseen linear superposition approximation, the

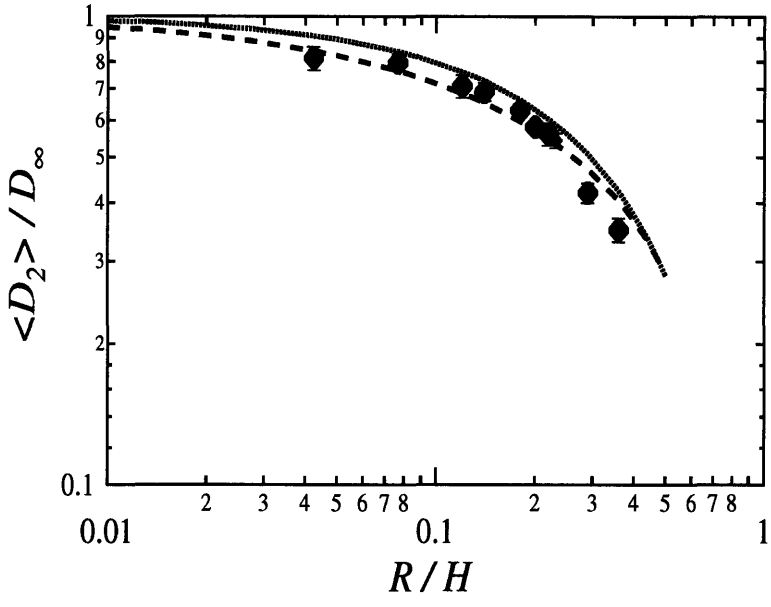

FIG. 5: Normalized gap-averaged diffusion coefficient versus normalized height of the channel for the beads. The dashed line represents the gap-averaged Oseen linear superposition approximation (equation 6) and the dotted line represents the non-averaged Oseen approximation (equation 5 with $z = H/2$).

Boltzmann distribution function was used to find the probability density function $P(z)$ in equation 6 [16]:

$$P(z) = \frac{1}{L_B}\left(\frac{e^{-\frac{z}{L_B}}}{e^{-\frac{R}{L_B}} - e^{-\frac{H-R}{L_B}}}\right) \tag{11}$$

$L_B = \frac{k_B T}{V(\rho_2 - \rho_1)g}$ is the characteristic length of the profile where ρ_2 is the density of the bead, ρ_1 is the density of the solvent, V is the volume of the sphere, and g is the gravitational acceleration. In our experiments, ρ_2 ~1.05g/mL and ρ_1 ~1.00g/mL. Since in all our experiments $L_B/H \geq 10$ (see Table I), equation 11 can be reduced to $P(z) \sim \frac{1}{H-2R}$. This probability distribution is a constant (step) function where all the locations between R and $H - R$ are equally likely.

From Figure 5 it can be seen that the gap-averaged Oseen linear superposition approximation agrees well with our experimental data to within experimental error. Figure 5 also shows a non-averaged Oseen approximation in which the bead is assumed to be at the midplane (equation 5 evaluated at $z = H/2$). Physically the bead diameter can not be larger than the height of the channel and therefore the beads can only be studied in the region

TABLE I: Table comparing the experimental bead data to the gap-averaged Oseen linear superposition approximation (equation 6) and the non-averaged Oseen approximation (equation 5 with $z = H/2$).

Radius (μm)	Channel Height (μm)	L_B/H	$\langle D_2 \rangle / D_\infty$	Error	Gap-Averaged Oseen	Non-Averaged Oseen
0.259	1.3	87	0.58	$\pm$0.01	0.57	0.63
0.259	2.1	54	0.71	$\pm$0.04	0.68	0.76
0.374	1.3	29	0.42	$\pm$0.02	0.47	0.51
0.374	2.1	18	0.63	$\pm$0.02	0.60	0.67
0.374	2.7	14	0.69	$\pm$0.03	0.66	0.73
0.463	1.3	15	0.35	$\pm$0.02	0.40	0.43
0.463	2.1	10	0.56	$\pm$0.03	0.55	0.60
0.055	1.3	9135	0.82	$\pm$0.05	0.85	0.91
0.161	2.1	225	0.80	$\pm$0.03	0.77	0.84

$R/H \leq 0.5$. At the point $R/H = 0.5$, the bead stays fixed at the mid-plane and therefore the gap-averaged Oseen approximation equals the non-averaged Oseen approximation at this point. Table I displays the numerical values of the bead experiments and their experimental error. The experimental error was found by dividing the data into five smaller groups and calculating the standard deviation. It can be seen that the gap-averaged Oseen approximation deviates from the experimental values in both the positive and negative directions and the deviation is within the experimental error of the beads. The non-averaged Oseen approximation however always underestimates the effect of the wall and the deviations from the experimental results are not within the experimental error. This underestimation is to be expected since the effect the wall is at its least when the bead is in the mid-plane (farthest away from the wall). We can conclude that gap-averaging the Oseen approximation is crucial in predicting the effect of the wall in our system. It is interesting to note that the Oseen linear superposition approximation is derived using a far field approach that theoretically should not be valid when the particle in very close to the wall. Figure 5 however shows that the Oseen approximation is valid even at high confinement.

The far field approach is valid for particles of any shape. Therefore since the gap-averaged Oseen linear superposition approximation is valid for spheres, theoretically there should be a form of the approximation that is valid for polymer chains. In order to test this hypothesis,

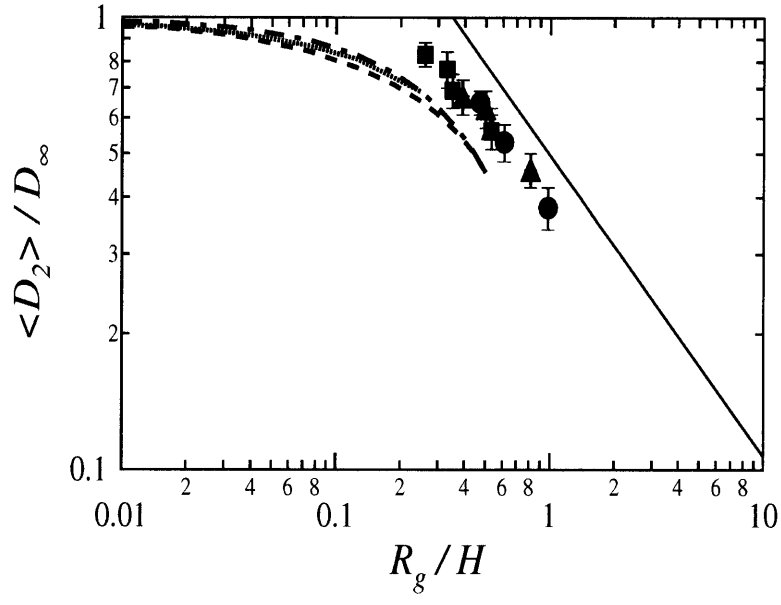

FIG. 6: Plot comparing DNA data to confined polymer and sphere theory. The experimental data for λ, 2-λ, and 3-λ DNA are represented by filled squares, triangles, and circles respectively. The solid line shows the $-\frac{2}{3}$ blob model scaling (equation 8), the dashed line is the scaled gap-averaged Oseen linear superposition approximation using R_g as the steric length (equation 12), the dotted line is the scaled gap-averaged Oseen approximation using $2R_g$ as the steric length, and the dot-dashed line is the non-averaged Oseen approximation (equation 5 with $z = H/2$).

the sphere radius R was replaced by the hydrodynamic radius R_h of DNA and the limits of integration in equation 6 were changed to the steric length of DNA, R_g:

$$\langle D_2 \rangle = \frac{1}{H - 2R_g} \int_{R_g}^{H-R_g} \frac{kT}{\xi_2(z)} dz \tag{12}$$

The relationship between the hydrodynamic radius and the radius of gyration was found by comparing the Zimm model (equation 10) to the Stokes-Einstein relation(equation 1):

$$R_g = \frac{6\pi 0.192}{\sqrt{6}} R_h \sim 1.48 R_h \tag{13}$$

The relationship between R_g and R_h was also found experimentally using free solution data for λ DNA. The experimental D_∞ was used to calculate R_h from the Stokes-Einstein relation and R_g was found from the second moment of the intensity distribution. This method yielded $R_g \sim 1.52 R_h$ which is to within 3% of that found by equation 13. Figure 6 shows a plot comparing the DNA data to both the blob theory (equation 8) and the scaled gap-averaged

Oseen approximation (equation 12). The figure shows that the scaled gap-averaged Oseen approximation underestimates the diffusivity of the DNA chains. To verify whether this discrepancy is due to underestimating the steric length of the molecule, the scaled gap-averaged Oseen approximation was also plotted using a larger steric length of $2R_g$. Increasing the steric length shifts the curve slightly up. The non-averaged Oseen approximation is also plotted (equation 5 with $z = H/2$). This non-averaged approximation represents an upper bound on the diffusivity since the effect the wall is the smallest when the DNA is in the mid-plane. Even the non-averaged Oseen approximation underestimates the diffusivity of the chains in the region of our data.

V. SUMMARY

We have used video microscopy and particle tracking to study the diffusion of both colloidal spheres and polymers in slit microchannels. Our molecules were not kept at a fixed height but instead were able to sample the entire gap. We found that it was necessary to gap-average the Oseen linear superposition approximation in order to get good agreement with our experimental bead data. Even though the Oseen approximation uses a far field approach, we found very good agreement even at very high confinement.

All our DNA experimental data was in the region $R_g/H > 0.25$. In this region of high confinement, a scaled Oseen linear superposition approximation was not valid and therefore the DNA diffusivity could not be modeled using a far field approach. When the DNA becomes strongly confined, the hydrodynamic interactions get screened and the coil transitions from nondraining to free draining. The blob model predicts that the diffusivity scaling in this highly confined region will be $\langle D_2 \rangle / D_\infty \sim (R_g/H)^{-\frac{2}{3}}$. We find good agreement with this scaling for our DNA data. This free draining behavior in the region $R_g/H > 0.25$ is in agreement with the simulations of Chen et al. [11]. It is probable that in the less confined region ($R_g/H < 0.1$), the chains can be modeled using the scaled Oseen linear superposition approximation since the far field approach is more valid in this region. This less confined region however was not studied since most of the current research in confined regions involves devices on the order of microns.

VI. REFERENCES

[1] G. C. Randall and P. S. Doyle, Phys. Rev. Lett. **93**, 058102 (2004).

[2] J. Han and H. G. Craighead, Science **228**, 1026 (2000).

[3] S. Mitragotri, J. Controlled Release **86**, 69 (2003).

[4] C. Janicki, C. Hwang, and E. R. Edelman, Medical Phys. **30**, 2622 (2003).

[5] M. R. Bennett, L. Farnell, W. G. Gibson, and D. Blair, J. Theoretical Biology **226**, 359 (2004).

[6] J. Happel and H. Brenner, *Low Reynolds Number Hydrodynamics* (Kluwer, Dordrecht, 1991).

[7] E. R. Dufresne, D. Altman, and D. G. Grier, Europhys. Lett. **53**, 264 (2001).

[8] L. Lobry and N. Ostrowsky, Phys. Rev. B **53**, 12050 (1996).

[9] B. Lin, J. Yu, and S. A. Rice, Phys. Rev. E **62**, 3909 (2000).

[10] F. Brochard and P. G. de Gennes, J. Chem. Phys. **67** (1977).

[11] Y.-L. Chen, M. D. Graham, J. J. de Pablo, G. C. Randall, M. Gupta, and P. S. Doyle, preprint (2004).

[12] R. M. Jendrejack, E. T. Dimalanta, D. C. Schwartz, M. D. Graham, and J. J. de Pablo, J. Chem. Phys. **119**, 1165 (2003).

[13] T. T. Perkins, D. E. Smith, and S. Chu, Science **276**, 2016 (1997).

[14] G. Randall and P. Doyle, preprint (2004).

[15] M. Doi and S. F. Edwards, *The Theory of Polymer Dynamics* (Clarendon Press, Oxford, 1986).

[16] L. P. Faucheux and A. J. Libchaber, Phys. Rev. E **49**, 5158 (1994).